analytical chemistry

pubs.acs.org/ac Article

Swing Arm Location-Controllable DNA Walker for Electrochemiluminescence Biosensing

Ni Liao, Mei-Chen Pan, Li Wang, Fan Yang, Ruo Yuan, and Ying Zhuo*

Cite This: *Anal. Chem.* 2021, 93, 4051−4058 Read Online

ACCESS | Metrics & More | Article Recommendations | Supporting Information

ABSTRACT: Here, we described a novel swing arm location-controllable DNA walker based on the DNA tetrahedral nanostructures (DTNs) for nucleic acid detection using the polycyclic aromatic hydrocarbon (PAH) microcrystals (TAPE-Pe MCs) consisting of the nonplanar molecular tetrakis(4-aminophenyl)ethene (TAPE) and planar molecular perylene (Pe) as electrochemiluminescence (ECL) luminophores. Specifically, the swing arm strands and track strands were fixed simultaneously on the DTNs to obtain the location-controllable DNA walker, which possessed an improved reaction efficiency compared to that of a fixed swing arm-based DNA walker due to the quantitative and orderly swing arm on the DTNs. On the other hand, the Pe microcrystals doped by TAPE molecules could decrease the $\pi-\pi$ stacking of Pe molecules for the ECL efficiency enhancement, achieving a blue-shifted and intense ECL emission. Therefore, we defined this enhanced and blue-shifted ECL phenomenon as "inhibition of conjugation-driven ECL (IC-ECL)". To prove these principles, a location-controllable DNA walker-based ECL biosensor was developed with microRNA let-7a as target molecules. The ECL biosensor achieved a low detection limit of 4.92 fM within a wide linear range from 10 fM to 100 nM. This approach offers a new insight for ECL efficiency increase and location-controllable strategies with improved reaction efficiency, demonstrating potential in diagnostic analysis.

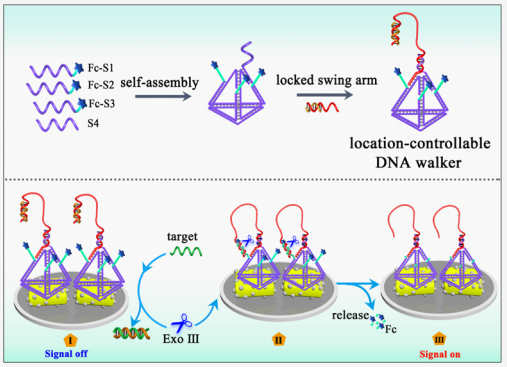

1. INTRODUCTION

DNA walkers are a kind of nanoscale molecular devices formed by swing arm strands and predetermined track strands, which can move autonomously along the preset orbit and further output the signals during the walking process.[1,2] Recently, they have drawn wide attention owing to their potential application in analytical and diagnostic fields because of their outstanding signal conversion.[3,4] In particular, the reported DNA walkers can be divided into two types according to the states of swing arm strands: (1) free swing arm strands and (2) fixed swing arm strands. For example, Chen's group[5] developed a DNA walker with target-triggered free swing arm strands, which could move automatically along DNA tracks assembled on the solid interface for the signal enhancement, realizing the electrochemical detection of exosomal microRNA-21 (MiR-21). However, the reaction between the swing arm strands and DNA tracks depended on the random collision of each other in homogeneous solution, which might be suspended due to the deviation from the orbit of the swing arm strands, resulting in the lower efficiency of DNA walkers. To overcome the above problems, Yu and his colleagues[6] have reported a fixed swing arm strand-based DNA walker, in which both of the swing arm strands and track strands were immobilized on the solid interface randomly, improving the collision efficiency and walking continuity. However, the relative location of the swing arm strands and track strands was still uncontrollable that led to the invalid collision and depressed reaction efficiency. In contrast, we believe that a DNA tetrahedral nanostructure (DTN)-based location-controllable strategy would be beneficial for the development of efficient DNA walkers due to the intrinsic nature of mechanical rigidity and well-controlled orientation,[7] achieving the regulatability of the relative location. Thus, a novel location-controllable strategy was developed in this work to regulate the relative location between swing arm strands and track strands based on DTN scaffolds for an efficient DNA walker construction, and little attention has been paid previously to this strategy.

Electrochemiluminescence (ECL) has aroused great interest by virtue of its high sensitivity, wide range, and low background signals.[8−10] Compared with traditional ECL emitters, such as luminol and $Ru(bpy)_3^{2+}$, polycyclic aromatic hydrocarbons (PAHs) and derivatives as ECL luminophores have received great attention for ECL bioanalysis and imaging over the past few decades due to their high fluorescence (FL) quantum efficiency, relatively low cost, and structural tailorability.[11−13] Perylene (Pe) is a PAH molecule with a

Received: December 2, 2020
Accepted: February 3, 2021
Published: February 15, 2021

https://dx.doi.org/10.1021/acs.analchem.0c05051
Anal. Chem. 2021, 93, 4051−4058

Scheme 1. Schematic Illustration of the Location-Controllable DNA Walker Fabrication (A), the Operating Principle of the Biosensor Based on the Location-Controllable DNA Walker for let-7a Determination (B), and Preparation of TAPE-Pe MCs (C)

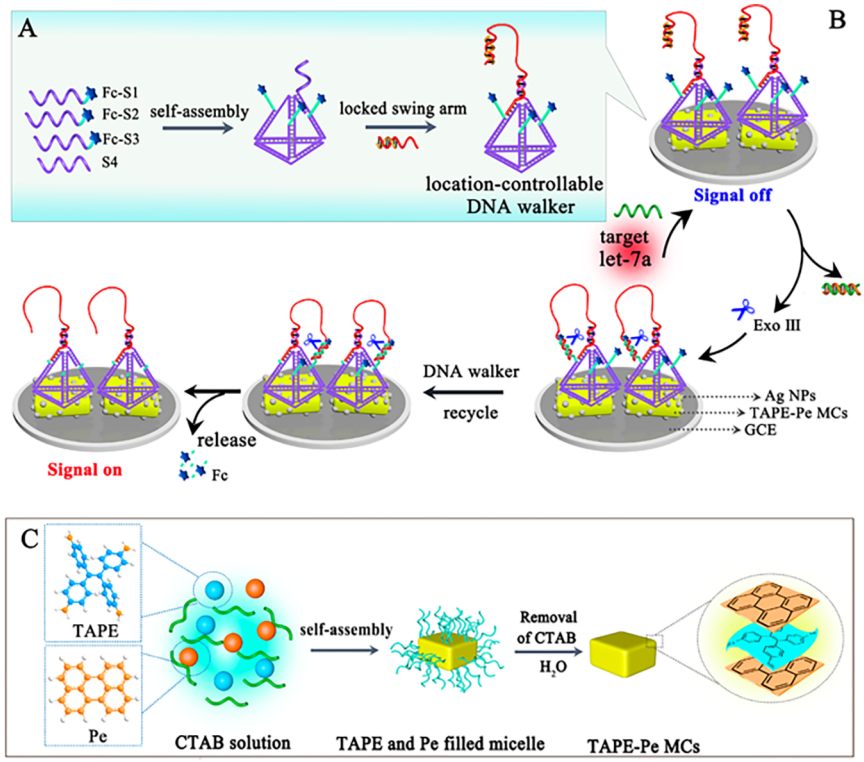

large π-conjugated structure, which has been extensively explored owing to its excellent photochemical properties. However, the unexpected aggregation-caused quenching (ACQ) effect was unavoidable when it was in solid or aggregated states, because Pe as a typical plane molecule was prone to form aggregates *via* intermolecular $\pi-\pi$ stacking, which will decrease their emission efficiency. Thus, much effort has been expended to reducing the ACQ of Pe by chemical modification of the skeleton of Pe at the bay positions. In a recent study, Zong et al.[14] introduced the rotatable aromatic rings on the core of the Pe diimide and achieved the conversion of luminescent molecules from ACQ to aggregation-induced emission (AIE). Tang's group[15] modified the bay area of a perylenediimide (PDI) core with tetraphenylethylene (TPE) to achieve a strong FL signal. Although the above works have achieved an enhanced FL response of the synthesized Pe derivatives by reducing the ACQ effect, there have been no reports on how to enhance the ECL of the originally non- or poor electrochemiluminescent PAHs in aqueous media so far. From this perspective, it was highly desirable to develop an efficient and convenient strategy to make coplanar PAH molecules avoid ACQ and emit a strong ECL signal.

In the current study, an economic and facile strategy was developed to minimize the ACQ of Pe through the doping of the nonplanar molecule with a propeller-shaped structure, tetrakis(4-aminophenyl)ethene (TAPE), into Pe microcrystals (Pe MCs) *via* $\pi-\pi$ stacking to generate the TAPE-Pe microcrystals (TAPE-Pe MCs), which achieved a significantly amplified ECL in an aqueous solution. As a proof-of-concept, a TAPE-Pe MC-based ECL sensing platform was developed in combination with a swing arm location-controllable DNA walker to detect microRNA let-7a (let-7a). As shown in Scheme 1A, the swing arm strands and track strands were fixed on the vertices and three edges of DTNs, respectively, to obtain the location-controllable DNA walker. Then, TAPE-Pe MCs and silver nanoparticles (Ag NPs) were assembled on a glassy carbon electrode (GCE) successively to immobilize the ferrocene (Fc)-labeled DNA walker *via* Ag−S bonds, achieving the "signal-off" state as the quenching effect of Fc. When the let-7a was present, the ECL intensity increased along with the process of DNA walking as Fc was getting released from the electrode surface with the help of the exonuclease III (Exo III). Furthermore, the proposed location-controllable strategy could increase the reaction efficiency and improve the kinetics of the DNA walkers, which could throw a new light on the sensitive detection of biomolecules in clinical bioanalysis.

2. EXPERIMENTAL SECTION

2.1. Synthesis of TAPE-Pe MCs. The preparation process of TAPE-Pe MCs is illustrated in Scheme 1C. First, 3.9 mg of TAPE and 2.5 mg of Pe were dispersed in 6.5 mL of "good" solvent (tetrahydrofuran, THF) under sonication to obtain a well-distributed mixture solution containing TAPE and Pe (with a TAPE/Pe mole ratio of 1:1). Then the resultant mixture solution was quickly added into 10 mL of "poor" solvent (deionized water containing 15 mmol/L hexadecyl trimethyl ammonium bromide) under stirring for 20 min. Finally, the TAPE-Pe MCs were purified three times with ethanol and deionized water alternately using centrifugation. Then, the TAPE-Pe MCs were redispersed in deionized water. The pure Pe microcrystals (Pe MCs) and the pure TAPE microcrystals (TAPE MCs) were prepared by a similar method (the preparation details are shown in the Section 1.3 of the Supporting Information).

https://dx.doi.org/10.1021/acs.analchem.0c05051
Anal. Chem. 2021, 93, 4051−4058

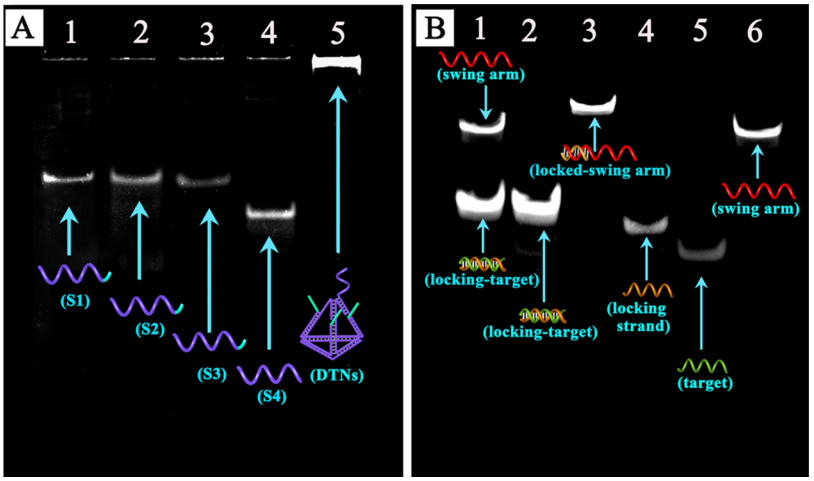

Figure 1. (A) PAGE analysis of the DTN self-assembly. lane 1, S1; lane 2, S2; lane 3, S3; lane 4, S4; and lane 5, the mixture of S1, S2, S3, and S4. (B) PAGE analysis of various samples. lane 1, the mixture of locking strands, target let-7a, and swing arm strands; lane 2, the mixture of locking strands and target let-7a; lane 3, the mixture of swing arm strands and locking strands; lane 4, locking strands; lane 5, target let-7a; and lane 6, swing arm strands. The concentration of 1 μM was chosen in the PAGE assay for all of the samples.

2.2. Preparation of the Location-Controllable DNA Walker. The location-controllable DNA walker was synthesized through the following steps. First, 100 μL of 20 mM S4 was activated by reducing disulfide bonds with 5 μL of tris-(2-carboxethyl)-phosphine hydrochloride (TCEP, 1 M) for 1 h. Second, equimolar quantities of S1, S2, S3, and S4 (the sequence information is shown in Section S1.1 of the Supporting Information, Table S1) were dispersed in the Tris−magnesium sulfate buffer (TM, 10 mM Tris−HCl and 50 mM $MgCl_2$, pH 8.0) at a final concentration of 2.0 μM. The resultant mixture solution was heated to 95 °C for 10 min and cooled down to 4 °C quickly for DTN generation. Third, 50 μL of the solution containing 2 μM locking strands and 2 μM swing arm strands were hybridized with each other at 37 °C for 120 min to obtain the locked swing arm products, which were hybridized with 50 μL of DTNs (2 μM) at 37 °C for 120 min to acquire the location-controllable DNA walker solution.

2.3. Preparation of the Proposed Biosensor. Initially, the bare GCE was polished with 0.05 μm Al_2O_3 powder. Subsequently, it was sonicated for further application. Ten microliters of poly(diallyldimethylammonium chloride) (PDDA, 4 wt % in water) was added into 1 mL of the TAPE-Pe MC solution to achieve the positively charged TAPE-Pe MCs. After that, 10 μL of TAPE-Pe MC solution was dropped onto the GCE surface to form the layer of TAPE-Pe MCs (TAPE-Pe MCs/GCE). Next, the Ag NP solution (10 μL) was dropped on the resultant electrode to obtain the Ag NP layer-modified TAPE-Pe MCs/GCE (Ag NPs/TAPE-Pe MCs/GCE) *via* electrostatic adsorption. After that, 10 μL of 1 μM location-controllable DNA walker solution was incubated on the resultant electrode for 6 h at 25 °C and further rinsed with phosphate buffer saline (PBS, pH 7.4). Eventually, the DNA walker/Ag NPs/TAPE-Pe MCs/GCE was passivated with hexanethiol (HT, 1.0 mM, ethanol) for 40 min to block the unoccupied sites.

2.4. Measurement Procedure. In brief, the target let-7a with various concentrations was added into the reaction solution (the total volume was 100 μL) containing 10 μL of 10× Exo III buffer and 1 μL of 500 U/μL Exo III. Then, the proposed biosensor was incubated with 10 μL of the mixture solution for 2 h at 37 °C. Then, to denature the enzymes, the resultant electrode was placed in a 90 °C oven for 10 min and rinsed with PBS (pH 7.4) to remove the unbound residues. Finally, the ECL response was measured with potentials from −2 to 0 V at 300 mV/s in 2 mL of detection solution (containing 10 mM $S_2O_8^{2-}$, pH 7.4) with the voltage of the high-voltage PMT maintained at 800 V.

3. RESULTS AND DISCUSSION

3.1. DTN Assembly and Feasibility Analysis of the DNA Walker. The native polyacrylamide gel electrophoresis (PAGE) assay was used to confirm the DTN generation and the feasibility of the location-controllable DNA walker response to target let-7a. As shown in Figure 1A, lanes of 1, 2, 3, and 4 loaded the S1, S2, S3, and S4, respectively. The PAGE image displayed a distinct single band on the respective lanes. Lane 5 loaded a mixture of S1, S2, S3, and S4, which exhibited a bright band at the top of the strip. It could be assigned to the hybridization of S1, S2, S3, and S4 that generated the DTNs, which possessed a large number of bases. As shown in Figure 1B, lane 1 loaded a mixture of locking strands, target let-7a, and swing arm strands, and the PAGE images displayed two distinct bands with a slower migration band (the top one) and a faster migration band (the bottom one). Herein, it can be inferred that the top one corresponded to the swing arm strands and the bottom one was attributed to the hybridization of the locking strands and target let-7a according to the experimental design. Furthermore, lane 2, which loaded a mixture of locking strands and target let-7a, exhibited a bright band with the same migration rate compared with that of the bottom one in lane 1, manifesting the hybridization of the locking strands and target let-7a once again. And lane 3 loaded a mixture of locking strands and swing arm strands, which exhibited a bright band with the lower migration rate compared with that of the individual swing arm strands (the top one in lane 1), demonstrating that the swing arm strands hybridized with the locking strands resulting in the products with generation of more bases. In addition, the single distinct bands assigned to the locking strands, target let-7a, and swing arm strands were observed in lanes 4, 5, and 6, respectively. They displayed different migrations, which reversed to the numbers of their bases. The

https://dx.doi.org/10.1021/acs.analchem.0c05051
Anal. Chem. 2021, 93, 4051−4058

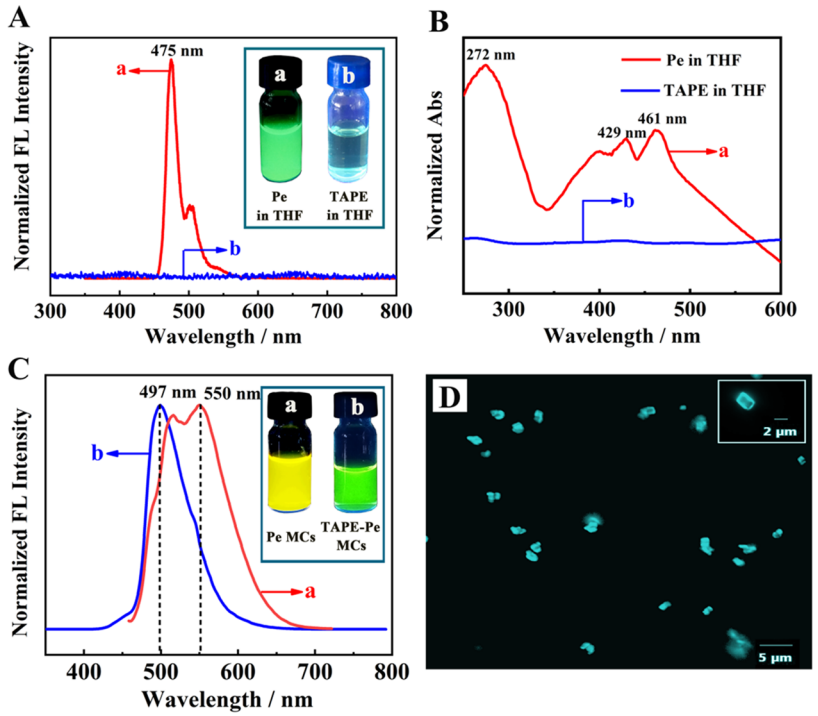

Figure 2. (A) FL emission peaks of Pe (curve a) and TAPE (curve b). Inset of A: images of Pe (a) and TAPE (b) dissolved in THF (under 365 nm UV light). (B) UV−vis absorption spectra of Pe (curve a) and TAPE (curve b) in THF. (C) FL emission peaks of the Pe MCs and TAPE-Pe MCs in deionized water. Inset of C: images of Pe MCs (a) and TAPE-Pe MCs (b) in deionized water under 365 nm UV light. (D) Pseudocolored FL microscopic image of the TAPE-Pe MCs.

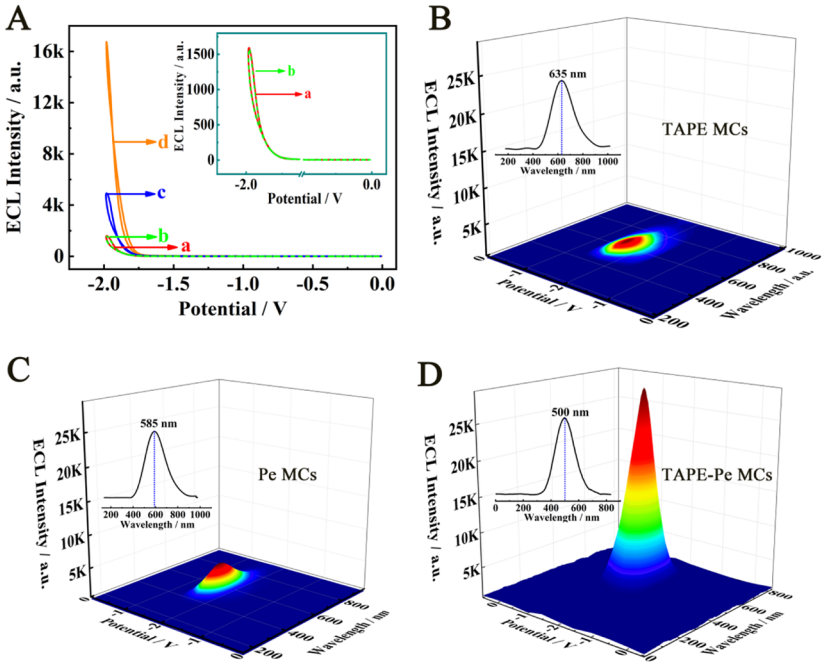

Figure 3. (A) ECL−voltage curves of bare GCE (curve a), TAPE MCs/GCE (curve b), Pe MCs/GCE (curve c) and TAPE-Pe MCs/GCE (curve d) in 2 mL of 10 mmol/L $S_2O_8^{2-}$ (pH 7.4). The ECL-voltage-wavelength of TAPE MCs (B), Pe MCs (C), and TAPE-Pe MCs (D) *via* a three-dimensional (3D) surface image.

results demonstrated that DTNs were formed successfully and the target could hybridize with the locked swing arm, resulting in the generation of the activated swing arm strands.

3.2. UV−Vis Absorption, FL Spectra, and Fluorescence Imaging Photographs of the TAPE-Pe MCs. The dispersed states of TAPE and Pe were obtained by dissolving the corresponding substances in an aprotic solvent (THF). The FL spectrum of Pe in THF was located at 475 nm (curve a, Figure 2A) and almost no FL emission peak of TAPE in THF was observed (curve b, Figure 2A). It was observed that the Pe molecule in the dispersed state has strong FL emission,[16] which could be attributed to the emission of the

https://dx.doi.org/10.1021/acs.analchem.0c05051
Anal. Chem. 2021, 93, 4051−4058

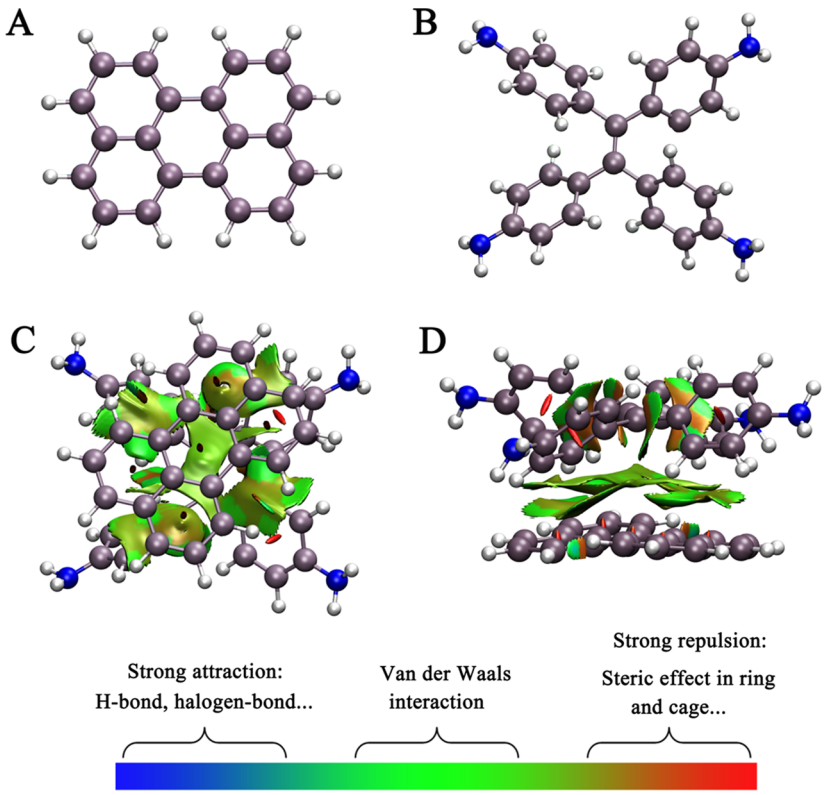

Figure 4. Molecular structures of Pe (A) and TAPE (B) and RDG analysis for TAPE and Pe (C, D).

excited monomer (^{1}Pe*), and the TAPE molecule has no FL emission under the excitation condition. Moreover, the images of Pe (a) and TAPE (b) in THF under 365 nm UV light are also demonstrated as the inset in Figure 2A. Furthermore, the UV−vis absorption spectra of Pe and TAPE in THF are shown in Figure 2B. Curve a is the UV−vis absorption spectrum of Pe, which displayed three characteristic absorption peaks at 272, 429, and 461 nm. Curve b is the UV−vis absorption spectrum of TAPE, which has no evident UV−vis absorption peak, demonstrating why the Pe molecule has strong FL emission compared to the TAPE molecule. In contrast, the aggregated states of TAPE and Pe were obtained by dissolving the corresponding microcrystals in a protic solvent (deionized water). As shown in Figure 2C, the FL emission peak of Pe MCs was located at 550 nm (curve a), and the corresponding image displayed a visible yellow fluorescence under 365 nm UV light (inset of Figure 2A), which could be assigned to the emission of the excited dimers or excimer (^{1}Pe$_2$*) due to the strong $\pi-\pi$ stacking effect of the coplanar molecule.[17] More importantly, the strongest FL emission peak of TAPE-Pe MCs was obtained at 497 nm, which was blue-shifted by about 53 nm compared with the strong FL peak of Pe MCs (550 nm). The corresponding image displayed a visible green fluorescence under 365 nm UV light in the inset of Figure 2C, which was similar to that of Pe in the dispersed states (inset of Figure 2A). The reason was that TAPE-Pe MCs doped by the TAPE molecules could suppress the aggregation and increase the monodispersity of Pe molecules. Besides, the FL microscopic images of TAPE-Pe MCs are shown in Figure 2D; the morphology and size of TAPE-Pe MCs in the fluorescence microscopic image were in accordance with the SEM images of TAPE-Pe MCs (as shown in Figure S1A of the Supporting Information).

3.3. ECL and ECL Spectrum Characteristics of the TAPE-Pe MCs. The ECL−voltage curves of the TAPE MCs, Pe MCs, and TAPE-Pe MC-modified GCE in 2 mL of $S_2O_8^{2-}$ solution (10 mM, pH 7.4) are illustrated in Figure 3A with a potential scan cycle from −2 to 0 V. The ECL−voltage curves of the bare GCE (curve a) and TAPE MCs/GCE (curve b) were almost overlapped, which could imply that both of the excited states were ascribed to emission of singlet oxygen [$^1(O_2)_2$*]. Compared with the ECL intensity of Pe MCs/GCE (5176 au, curve c), the ECL intensity of TAPE-Pe MCs MCs/GCE was amplified by 3.5-fold (18 1 05 au, curve d). It can be inferred that Pe microcrystals doped by the TAPE molecules could suppress the aggregation of Pe molecules and enhance the ECL emission of Pe significantly. As shown in Figure 3B, the ECL spectrum of TAPE MCs/GCE was observed at 635 nm in $S_2O_8^{2-}$ solution, which had the same ECL spectrum location as that of the GCE in $S_2O_8^{2-}$ (in the Section S1.6 of the Supporting Information), confirming that the excited states of both TAPE MCs/GCE and the bare GCE in $S_2O_8^{2-}$ solution were the $^1(O_2)_2$*[18] and the TAPE MCs had no ECL response in the potential range of −2 to 0 V. In contrast to that of TAPE MCs, the ECL spectrum of Pe MCs was at 585 nm (Figure 3C) due to the ECL emission of the excited Pe dimers or excimer in Pe MCs. The ECL spectrum of TAPE-Pe MCs was observed at 500 nm (Figure 3D), which exhibited a blue shift and the change trend was consistent with FL emission of TAPE-Pe MCs compared with Pe MCs. Furthermore, in comparison with that of pure Pe MCs, it was found that the relative ECL efficiency of the TAPE-Pe MCs was enhanced by 178% (detailed calculation is provided in Supporting Information Section S1.9). The results demonstrated that the Pe microcrystals doped by TAPE molecules could enhance the ECL efficiency and achieve a

https://dx.doi.org/10.1021/acs.analchem.0c05051
Anal. Chem. 2021, 93, 4051−4058

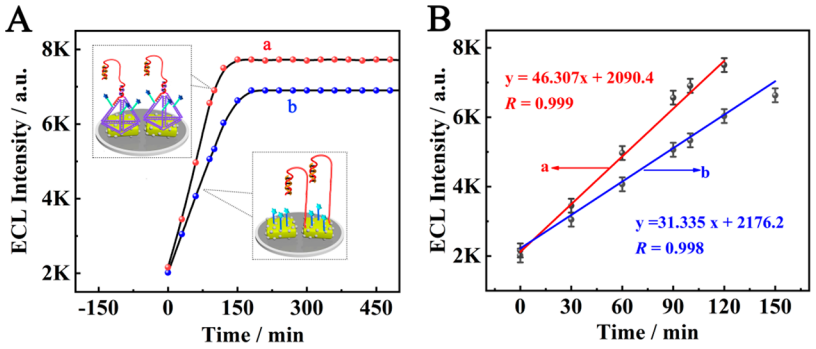

Figure 5. (A) ECL intensity profiles of the as-proposed biosensor (HT/location-controllable DNA walker/Ag NPs/TAPE-Pe MCs/GCE) (curve a) and the contrasting biosensor (HT/fixed swing arm/Fc-DNA/Ag NPs/TAPE-Pe MCs/GCE) (curve b) toward target let-7a. (B) ECL initial movement rate of the designed location-controllable swing arm-based biosensor (curve a) and the fixed swing arm-based biosensor (curve b) toward target let-7a.

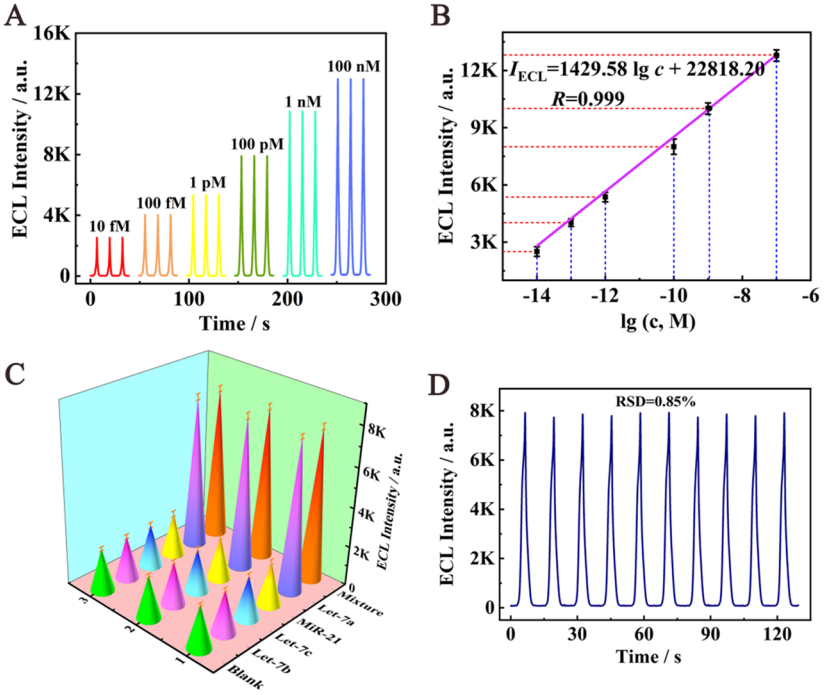

Figure 6. (A) ECL response curves of the constructed biosensor to detect let-7a with different concentrations: 1.0×10^{-14}, 1.0×10^{-13}, 1.0×10^{-12}, 1.0×10^{-10}, 1.0×10^{-9}, and 1.0×10^{-7} M. (B) Calibration curve for the linear relation between the ECL intensity and the logarithm of let-7a concentrations. (C) Selectivity of the designed biosensor with different agents. (D) Stability of the designed biosensor with 100 pM let-7a.

blue-shifted and intense ECL emission. Therefore, we defined this enhanced and blue-shifted ECL phenomenon as "inhibition of conjugation-driven ECL (IC-ECL)".

3.4. Quantum Chemistry for TAPE and Pe. Figure 4A,B displays the configuration of Pe and TAPE, respectively. It could be seen that the Pe molecule has a two-dimensional planar structure, and the TAPE molecule shows a nonplanar propeller-shaped structure. A reduced density gradient (RDG) analysis[19,20] was employed to confirm the noncovalent interactions between TAPE and Pe in the TAPE-Pe MCs. As shown in Figure 4C,D, a blue-green-red scale based on the values of sign($\lambda 2$)*ρ was selected to color the gradient isosurfaces. The green regions of the isosurfaces indicated the $\pi-\pi$ interaction and the spikes in red color indicated the steric effect between TAPE and Pe. Thus, it was confirmed that the TAPE molecule with the propeller-shaped structure might possess large steric hindrance, which could decrease the $\pi-\pi$ stacking of Pe molecules, resulting in the change of the state of Pe molecules from aggregates to the corresponding monomers in the microcrystals. The above results provided the theoretical support for the "IC-ECL" phenomenon.

3.5. Comparison of the Reaction Efficiency with Different DNA Walker Strategies. To demonstrate the efficiency of the location-controllable DNA walker strategy, typical kinetic data of the proposed swing arm-based biosensor and a fixed swing arm-based biosensor were studied under the same experimental conditions. And schematic diagrams of the fabrication process of the proposed swing arm-based and randomly fixed swing arm-based biosensors are shown in insets a and b of Figure 5A, respectively. The ECL response of the fixed swing arm-based biosensor showed an upward trend with increasing reaction time, and the ECL intensity approached a balance point after 150 min (curve b). However, the higher ECL intensity of the proposed DNA walker strategy was obtained within a shorter time (120 min, curve a). As displayed in Figure 5B, the reaction time within 120 and 150 min fitted

https://dx.doi.org/10.1021/acs.analchem.0c05051
Anal. Chem. 2021, 93, 4051−4058

to linear equations of $y = 46.307x + 2090.4$ and $y = 31.335x + 2176.2$ (where y represents ECL intensity, x represents the reaction time, and the slope represents the reaction rate), and the correlation coefficients were 0.999 and 0.998, respectively. The above results demonstrated that the proposed swing arm-based biosensor toward target let-7a possessed a larger reaction rate (k_a = 46.307) compared with the randomly fixed swing arm-based biosensors (k_b = 31.335).

3.6. Analytical Performance of the Biosensor. The analytical application of the constructed biosensor was implemented for the detection of let-7a under the optimal conditions. The ECL intensity of the biosensor increased with the concentration of let-7a increasing from 1.0×10^{-14} to 1.0×10^{-7} M (Figure 6A). Moreover, there was a linear relation between the ECL intensity (I_{ECL}) and the logarithmic value of let-7a concentrations ($\lg c$). The regression equation was $I = 1429.58 \lg c + 22\,818.2$, and the detection limit was as low as 4.92 fM (Figure 6B).

To evaluate the practicality and specificity, the selectivity of constructed biosensors for let-7a detection was investigated. Different interfering agents, such as microRNA let-7b (let-7b), microRNA let-7c (let-7c), and MiR-21, at the concentration of 1 nM were explored to test with the biosensor instead of let-7a (100 pM). As depicted in Figure 6C, the ECL response of the developed biosensor toward the interfering agents at high concentrations exhibited no obvious difference compared with that of the blank sample. Moreover, a mixed solution containing let-7b (1 nM), let-7c (1 nM), MiR-21 (1 nM), and let-7a (100 pM) was selected to test the developed biosensor. The ECL response of the biosensor exhibited no distinct difference from that of the standard let-7a (100 pM) only case. And the results demonstrated that the developed ECL strategy possessed an extraordinary selectivity to detect let-7a. Figure 6D displays the satisfactory stability of the as-proposed ECL biosensor, where the ECL response of the biosensor with 100 pM let-7a remained stable within 10 cycles and the relative standard deviation (RSD) was 0.85%.

4. CONCLUSIONS

We have reported a new location-controllable DNA walker strategy combined with the intense ECL platform of TAPE-Pe MCs for let-7a detection. Significantly, TAPE-Pe MCs exhibited the inhibition of conjugation-driven ECL (IC-ECL) emission with enhanced ECL efficiency compared with the pure Pe MCs, thanks to the reduction of the ACQ effect by the doping of TAPE molecules with the nonplanar propeller-shaped structure. Moreover, the location-controllable strategy could regulate the relative location of swing arm strands and track strands, further decrease uneven distribution, and improve the reaction efficiency. The proposed location-controllable DNA walker-based biosensor toward target let-7a showed a limit of detection as low as 4.92 fM, which provided a promising modular platform for bioanalysis.

■ ASSOCIATED CONTENT

Supporting Information

The Supporting Information is available free of charge at https://pubs.acs.org/doi/10.1021/acs.analchem.0c05051.

Reagents and materials; apparatus; preparation of the pure Pe MCs and TAPE MCs; preparation of Ag nanoparticles (Ag NPs); microstructure and zeta potential characterization of various nanomaterials; images of Pe and TAPE with different states and the ECL spectrum of $S_2O_8^{2-}$; ECL and electrochemical impedance spectroscopy (EIS) characterizations of the proposed biosensor; optimization of the reaction conditions; and the relative ECL efficiency of TAPE-Pe MCs (PDF)

■ AUTHOR INFORMATION

Corresponding Author

Ying Zhuo − *Key Laboratory of Luminescence Analysis and Molecular Sensing (Southwest University), Ministry of Education, College of Chemistry and Chemical Engineering, Southwest University, Chongqing 400715, China;* orcid.org/0000-0002-4491-1186; Phone: +86 23 68253172; Email: yingzhuo@swu.edu.cn

Authors

Ni Liao − *Key Laboratory of Luminescence Analysis and Molecular Sensing (Southwest University), Ministry of Education, College of Chemistry and Chemical Engineering, Southwest University, Chongqing 400715, China; College of Biological and Chemical Engineering, Panzhihua University, Panzhihua 617000, China*

Mei-Chen Pan − *Key Laboratory of Luminescence Analysis and Molecular Sensing (Southwest University), Ministry of Education, College of Chemistry and Chemical Engineering, Southwest University, Chongqing 400715, China*

Li Wang − *Key Laboratory of Luminescence Analysis and Molecular Sensing (Southwest University), Ministry of Education, College of Chemistry and Chemical Engineering, Southwest University, Chongqing 400715, China*

Fan Yang − *Key Laboratory of Luminescence Analysis and Molecular Sensing (Southwest University), Ministry of Education, College of Chemistry and Chemical Engineering, Southwest University, Chongqing 400715, China*

Ruo Yuan − *Key Laboratory of Luminescence Analysis and Molecular Sensing (Southwest University), Ministry of Education, College of Chemistry and Chemical Engineering, Southwest University, Chongqing 400715, China;* orcid.org/0000-0003-3664-6236

Complete contact information is available at: https://pubs.acs.org/10.1021/acs.analchem.0c05051

Notes

The authors declare no competing financial interest.

■ ACKNOWLEDGMENTS

This work was financially supported by the NNSF of China (22022408), the Chongqing Talents Personnel Support Program (CQYC201905067), and the Fundamental Research Funds for the Central Universities (XDJK2019TJ002).

■ REFERENCES

(1) Zhang, H.; Xu, X. W.; Jiang, W. *Chem. Sci.* **2020**, *11*, 7415−7423.
(2) Lv, M. M.; Liu, J. W.; Yu, R. Q.; Jiang, J. H. *Chem. Sci.* **2020**, *11*, 10361−10366.
(3) Jung, C.; Allen, P. B.; Ellington, A. D. *Nat. Nanotechnol.* **2016**, *11*, 157−163.
(4) Zhang, Y.; Zhang, X.; Li, Y. Y.; He, Y. L.; Liu, Y.; Ju, H. X.; Zhang, Y. *Chem. Sci.* **2020**, *11*, 6289−6296.
(5) Zhang, J.; Wang, L. L.; Hou, M. F.; Xia, Y. K.; He, W. H.; Yan, A.; Weng, Y. P.; Zeng, L. P.; Chen, J. H. *Biosens. Bioelectron.* **2018**, *102*, 33−40.

(6) Wang, K.; He, M. Q.; Zhai, F. H.; Wang, J.; He, R. H.; Yu, Y. L. *Biosens. Bioelectron.* **2018**, *105*, 159−165.
(7) Qing, Z. H.; Hu, J. L.; Xu, J. Y.; Zou, Z.; Lei, Y. L.; Qing, T. P.; Yang, R. H. *Chem. Sci.* **2020**, *11*, 1985−1990.
(8) Liu, Z.; Qi, W.; Xu, G. *Chem. Soc. Rev.* **2015**, *44*, 3117−3142.
(9) Voci, S.; Goudeau, B.; Valenti, G.; Lesch, A.; Jović, M.; Rapino, S.; Paolucci, F.; Arbault, S.; Sojic, N. *J. Am. Chem. Soc.* **2018**, *140*, 14753−14760.
(10) Tan, X.; Zhang, B.; Zou, G. Z. *J. Am. Chem. Soc.* **2017**, *139*, 8772−8776.
(11) Ko, S. H.; Lee, T.; Park, H. J.; Ahn, D. S.; Kim, K.; Kwon, Y.; Cho, S. J.; Ryoo, R. *J. Am. Chem. Soc.* **2018**, *140*, 7101−7107.
(12) Zou, Y.; Bonal, V.; Quintero, S. M.; Boj, P. G.; Villalvilla, J.; Quintana, J.; Li, G. W.; Wu, S. F.; Jiang, Q.; Ni, Y.; Casado, J.; Díaz-García, M.; Wu, J. S. *Angew. Chem., Int. Ed.* **2020**, *59*, 14927−14934.
(13) Liu, J. L.; Zhang, J. Q.; Tang, Z. L.; Zhuo, Y.; Chai, Y. Q.; Yuan, R. *Chem. Sci.* **2019**, *10*, 4497−4501.
(14) Zong, L. Y.; Zhang, H. Q.; Li, Y. Q.; Gong, Y. B.; Li, D. Y.; Wang, J. Q.; Wang, Z.; Xie, Y. J.; Han, M. M.; Peng, Q.; Li, X. F.; Dong, J. F.; Qian, J.; Li, Q. Q.; Li, Z. *ACS Nano* **2018**, *12*, 9532−9540.
(15) Zhao, Z.; Gao, S. M.; Zheng, X. Y.; Zhang, P. F.; Wu, W. T.; Kwok, R. K.; Xiong, Y.; Leung, N. C.; Chen, Y. C.; Gao, X. K.; Lam, J. Y.; Tang, B. Z. *Adv. Funct. Mater.* **2018**, *28*, No. 1705609.
(16) Suk, J. D.; Wu, Z. Y.; Wang, L.; Bard, A. J. *J. Am. Chem. Soc.* **2011**, *133*, 14675−14685.
(17) Wang, P.; Wu, Y. Y.; Wu, J.; Wang, S.; Yu, L.; Zhu, Q. Y.; Dai, J. *J. Mater. Chem. C* **2013**, *1*, 7973−7978.
(18) Wang, C. C.; Wang, H. M.; Fan, M. F.; Fei, L.; Luo, X. L.; Feng, J. J.; Yuan, P. X.; Wang, A. J. *Sens. Actuators, B* **2019**, *290*, 203−209.
(19) Priscillaa, J.; Dhas, D. A.; Joec, I. H.; Balachandrand, S. *Chem. Phys.* **2020**, *536*, No. 110827.
(20) Li, G. C.; Huang, L.; Yi, X. F.; Peng, Y. K.; Tsang, S. E.; Zheng, A. *Chem. Commun.* **2018**, *54*, 13435−13438.

https://dx.doi.org/10.1021/acs.analchem.0c05051
Anal. Chem. 2021, 93, 4051−4058